nature geoscience

SUPPLEMENTARY INFORMATION

DOI: 10.1038/NGEO2798

Global climate forcing of aerosols embodied in international trade

Jintai Lin, Dan Tong, Steven Davis, Ruijing Ni, Xiaoxiao Tan, Da Pan, Hongyan Zhao, Zifeng Lu, David Streets, Tong Feng, Qiang Zhang, Yingying Yan, Yongyun Hu, Jing Li, Zhu Liu, Xujia Jiang, Guannan Geng, Kebin He, Yi Huang, Dabo Guan

Table of Contents

Supplementary Information Methods

S1. Production-based emissions

Emissions of species other than NH_3

Production-based emissions represent pollutants physically released in each region, and they are calculated as the product of emission factors and activity rates. A country-specific E_p inventory in 2007 for SO_2, NO_x, CO, BC and POA is built for this study. The inventory uses a detailed technology-based methodology as in previous studies[32-34], and it covers 65 sectors and 228 countries/regions worldwide. Global anthropogenic emissions in 2007 are estimated at 101.7 Tg for SO_2, 95.3 Tg for NO_x, 532.1 Tg for CO, 5.8 Tg for BC, and 28.8 Tg for POA. [Here emitted POA is 2.1 times as much as organic carbon, after accounting for the oxygen atoms contained, consistent with the assumption in GEOS-Chem.] After the emission data are derived, they are further mapped to the 129 countries/regions and 57 sectors defined in the Global Trade Analysis Project version 8 (GTAP8)[24], in order to facilitate the subsequent calculation of consumption-based emissions. Emission factors and activity data are described as follows.

Activity data: We take the country-based fuel consumption data from the International Energy Agency (IEA)[35,36] for 46 sub-sectors and 51 fuels in four major sectors (residential, industry, power, and transportation). We further aggregate these fuels into 19 types, considering that emissions related to certain fuels in the IEA database are small and their emission factors are not available[27,32]. For Greenland, there

are no fossil fuel data in the IEA database, thus we use the data compiled in the United States Energy Information Administration (http://www.eia.gov/). We then divide the fuel use in each sector by different technologies (four technologies in the power sector, 10 in industry, 21 in transportation, and 11 in the residential sector)[32-34,37]. The technology distributions for various vehicle types follow previous studies[38,39]. Biofuel combustion technologies in the residential sector follow the Greenhouse Gas and Air Pollution Interactions and Synergies (GAINS, http://gains.iiasa.ac.at/models/) model. In addition, we include 16 non-combustion industrial process sectors, taking production data from the United States Geological Survey statistics (USGS, http://minerals.usgs.gov/minerals/pubs/myb.html) and United Nations data (UNdata, http://data.un.org/).

Emission factors: We compile emission factors from a wide variety of literature and our previous works, including using data from reliable regional inventories to calibrate the emission factors for China, India, Southeast Asia, Canada, the United States, and Europe. Emission factors for SO_2 from fuel combustion follow our previous works[27,40-43]. For the non-combustion sources, we take the unabated SO_2 emission factors from the public databases[44,45], and then we follow our previous studies[27,37,41,42] to employ the flue gas desulfurization application rates and corresponding SO_2 removal efficiencies. We use regional emission inventories[27,37,40,46,47] to calibrate the SO_2 emission factors for China, India, Southeast Asia, Canada, the United States, and Europe. Emission factors of NO_x and CO follow Yan et al.[39] for on-road vehicles and several public databases[44,45,48] for other sources; we further replace the global defaults

by regional emission databases where available[33,49-53]. For BC and POA, we take the emission factors from Bond et al.[32,54], except that we follow Yan et al.[38,39] for on-road vehicles, Lam et al.[55] and Huang et al.[56] for residential kerosene, and our previous works[27,46] for all emission factors of China and India.

Emissions of NH_3

An additional country-based E_p data base is built here for NH_3 in 2007. Emissions are calculated for 129 countries/regions and 57 sectors (13 for agricultural activities) defined in GTAP8[24]. We combine the global EDGAR inventory and several existing regional inventories that often have more detailed sectoral information to facilitate a global supply chain analysis (see Supplementary Information Table 2). For example, although agriculture accounts for 96% of global anthropogenic NH_3 emissions, there are 2–3 agricultural sectors only in EDGAR and other global inventories, whereas much more information is available in the regional inventories for the United States, China, and Europe. For regions other than the United States, China and Europe, agricultural emissions are often sorted in the inventories according to sources (e.g. fertilizer, compost, and manure) instead of sectors. In this case, we map the source-based emissions to individual agricultural sectors, using as weighting functions the regionally aggregated (over regions other than China, the US, and Europe) contributions of individual agricultural sectors from MASAGE.

Comparison with HTAP v2.2

The scatterplot in Supplementary Information Fig. 2 compares the E_p inventory built here with the HTAP v2.2 inventory for 2008[57]. HTAP v2.2 was recently developed from an internationally collaborative project, and it combines the EDGAR inventory[58] with regional inventories in Asia, North America, and Europe. HTAP v2.2 is thus expected to be more updated than EDGAR and other older global inventories. Supplementary Information Fig. 2 shows that total E_p emissions in our inventory are in line with HTAP v2.2. Our inventory is spatially consistent with HTAP v2.2 with a correlation coefficient of 0.99–1.00 for all the six species. The bias relative to HTAP v2.2 is within 8% for NO_x, CO, SO_2 and NH_3, 11% for BC, and 18% for POA. The differences for China, India, the United States and other large emitters are generally small. Although the differences are larger for small emitters, as expected, they are normally within the uncertainty of current emission inventories[2,59]. The E_p are very small for Greenland (the outlier region shown in the left of each panel), but the values here are much higher than HTAP v2.2; this is because the IEA fuel database for Greenland used in HTAP v2.2 contains missing values for fossil fuels, which issue is corrected here by taking the EIA data.

S2. Consumption-based emissions

Consumption-based emissions represent pollutants released along the global supply chain as a result of certain region's consumption of final products and services. For example, a cell phone purchased in the United States may be assembled in China with iron ores mined in Australia, Steel made in Japan and high-end assembling

mechanics manufactured in the United States. And consumption-based emissions attribute the pollutants consequently released in these countries to the United States.

Here we use the multi-regional input-output model (MRIO) from GTAP8[24], based on monetary flows, to trace the economic interconnections among sectors and regions. We then combine the MRIO analysis with the production-based emission inventory to obtain the consumption-based emissions on a country and sectoral basis. The above method has been used to calculate consumption-based emissions of CO_2 and air pollutants[15,20,21,60-63], and used to evaluate export-related environmental and health impact[13,26]. Detailed descriptions of the MRIO approach are provided in previous studies[18,21,60]. Below is a brief introduction of this approach.

$$\mathbf{x} = \mathbf{A}\mathbf{x} + \mathbf{y} = (\mathbf{I} - \mathbf{A})^{-1}\mathbf{y} \quad (1)$$

$$\mathbf{E}' = \hat{\mathbf{f}}(\mathbf{I} - \mathbf{A})^{-1}\mathbf{y}' \quad (2)$$

Equation 1 shows how final consumption is supplied through the supply chain across 129 countries and 57 sectors. Here $\mathbf{x}$ is a vector for country- and sector-specific monetary outputs to supply the associated final consumption $\mathbf{y}$ (e.g., supplied by any given country and sector to all countries and sectors), $\mathbf{A}\mathbf{x}$ is the intermediate outputs, $(\mathbf{I} - \mathbf{A})^{-1}$ is the Leontief inverse matrix, $\mathbf{A}$ is the direct requirement coefficient matrix, and $\mathbf{I}$ is the unit matrix. Equation 2 calculates region- and sector-specific consumption-based emissions $\mathbf{E}'$ associated with final consumption $\mathbf{y}'$ (e.g., supplied by all countries and sectors to any given country and sector). Here $\hat{\mathbf{f}}$ is the diagonalization of a vector representing region- and sector-explicit emissions per monetary output, as derived by dividing production-based emissions by monetary

outputs $\mathbf{x}$. Values of $\mathbf{y}$, $\mathbf{y}'$ and $\mathbf{A}$ are available in the MRIO model, and region- and sector-explicit production-based emissions are derived in this study.

S3. Gridded monthly emissions

Gridded emissions are required to drive the chemical transport modeling. We convert the country-based annual emissions to a monthly 0.1º long. x 0.1º lat. gridded dataset, based on the horizontal and monthly distribution of the HTAP v2.2 emission inventory for 2008[57]. To support the atmospheric simulations, in the model world, E_c of any region is released in countries producing goods to supply that region – for example, a portion of China's emissions is related to consumption in Western Europe, and in simulating the effect of E_c of Western Europe, this portion is released within the Chinese territory and is gridded following China's E_p. Supplementary Fig. 3 gives an example of how Western Europe's E_p and E_c of BC are distributed horizontally.

Prior to the conversion, we map our emissions from 57 sectors to five main sectors designated in HTAP v2.2 (power generation, industry, transportation, residential use, and agriculture).

S4. Atmospheric evolution and transport simulated by GEOS-Chem

We use the global GEOS-Chem CTM version 9-02 to simulate the atmospheric evolution of aerosols and precursor gases. A series of model simulations are conducted to derive the individual effects of E_p and E_c of the 11 aggregated regions on the atmospheric distribution of SIOA, POA and BC.

GEOS-Chem is driven by the GEOS-5 assimilated meteorology from the NASA Global Modeling and Assimilation Office (GMAO). The model is run on a 2.5º long. x 2º lat. grid with 47 vertical layers, with full O_x-NO_x-VOC-CO-HO_x gaseous chemistry[64,65] and online aerosol calculations. Simulated aerosols include SIOA[66,67], POA, BC[67,68], dust[69,70], and sea salts[71,72]. POA is simulated as primary organic carbon with less mass by a factor of 2.1; the remaining mass accounts for the oxygen molecules contained[73]. SIOA is assumed to be in thermodynamical equilibrium following ISOROPIA-II[74]. Wet scavenging of soluble aerosols and gases in convective updrafts, rainout, and washout follows Liu et al.[75], with updates for BC by Wang et al.[76]. Dry deposition of gases and aerosols follow Wesely[77] and Zhang et al.[78], respectively. Model advection uses the TPCORE algorithm of Lin and Rood[79], convection follows a modified Relaxed Arakawa-Schubert scheme[80], and mixing in the boundary layer follows a non-local scheme[81,82].

Global anthropogenic emissions of NO_x, SO_2, NH_3, CO, BC and POA are derived in this study. Other emissions are set as follows. Global anthropogenic emissions of non-methane volatile organic compounds (NMVOC) are taken from the RETRO dataset for 2000 as described by Hu et al.[83]; emissions in China, the rest of Asia and the United States are further replaced by the regional inventories MEIC for 2008 (www.meicmodel.org), INTEX-B for 2006[35] and NEI05 for 2005 (ftp://aftp.fsl.noaa.gov/divisions/taq/emissions_data_2005), respectively. Biogenic emissions of NMVOC follow the MEGAN model[84]. Soil emissions of NO_x follow Hudman et al.[85]. Lightning emissions of NO_x follow the Price and Rind scheme with a

satellite-based adjustment and a backward 'C-shape' vertical profile[86-88]. Biomass burning emissions use the monthly GFED-3 data for 2007[89].

We conduct three sets of model simulations for 2007 with a spin-up period of 6 months. The first set contains a control simulation (S1) with all emissions unperturbed and a second simulation (S2) with anthropogenic emissions of NO_x, SO_2, NH_3, CO, BC and POA removed globally. The second set of simulations (S3 to S13) tests the contributions of production-based emissions from the 11 regions, by removing anthropogenic emissions produced within their territories, one region at a time. The third set of simulations (S14 to S24) is the counterpart of the second set. It turns off global anthropogenic emissions related to consumption of each of these 11 regions. For each simulation, GEOS-Chem outputs 3-hourly 3-dimensional mass concentrations of SIOA, POA and BC for further radiative forcing calculations.

S5. Radiative forcing calculations using RRTMG

We use the RRTMG RTM for shortwave (RRTMG_SW version v3.9)[90] to calculate the all-sky top-of-the-atmosphere RF of SIOA, POA and BC, based on the atmospheric distributions of aerosols simulated by GEOS-Chem. The RF accounts for scattering and absorption of solar radiation in the atmosphere, i.e., the RF from aerosol-radiation interactions. It does not account for rapid adjustments or feedbacks of clouds and the hydrological cycle. The longwave RF is negligible[73] and not calculated here. Aerosols are assumed to mix externally to facilitate a species-specific RF calculation, and each aerosol type has a prescribed dry size distribution. Aerosol microphysical properties follow Heald et al.[73], including dry size distributions, hygroscopic growth

factors, and refractive indices. Following Hansen et al.[3], we further scale the RF of BC by a factor of two to account for enhanced absorption by internal mixing with other aerosols[2-4].

The spatially and temporally varying aerosol mass concentrations are obtained from the GEOS-Chem outputs. Ancillary meteorological and surface albedo data are taken from the GEOS-5 dataset, including cloud fraction, liquid water content, ice water content, air temperature, relative humidity, tropopause pressure, and air pressure profiles. The effective droplet radius is assumed as 14.2 μm for liquid clouds and 24.8 μm for ice clouds[73].

Three sets of RTM calculations, with a total of 70 runs, are conducted for 2007 in correspondence to the sets of CTM simulations. The first set contains a run (R1) including all anthropogenic aerosols globally and three subsequent runs (R2–R4) that are similar to R1 but removing global anthropogenic SIOA, POA and BC one by one. The second and third sets contain 33 (3 species x 11 regions per species) runs each, in which an aerosol species related to a given region's production or consumption is removed. To reduce the computational costs, the 3-hourly CTM aerosol data are averaged for each month to produce monthly mean 3-hourly datasets (i.e., the monthly mean diurnal cycle is preserved). The difference in RF between this monthly-mean based calculation and a calculation based on daily data is very small, according to our initial test.

The change from Ri (i = 2 to 70) to R1 gives the RF of an aerosol species globally (i = 2 to 4), related to a region's production (RF_p, i = 5 to 37), or related to a region's

consumption (RF_c, i = 38 to 70). For any aerosols (SIOA, POA and BC), the globally cumulated RF responds quite linearly to emission perturbations, as revealed by the fact that the RF_c is the same as the RF_p if the contributions of all regions are summed (Supplementary Information Table 1). The RF of SIOA contributed by individual regions may respond more nonlinearly to emission perturbations due to changes in the atmospheric oxidative capacity, dependence of sulfate and nitrate formation on the amount of NH_3[91], and additional nonlinearity in radiative transfer calculation. This nonlinearity is reduced here since emissions of all species are perturbed simultaneously in the CTM simulations, including CO that affects the oxidative capacity.

S6. Uncertainties and limitations

Our estimated global RF_p and RF_c (summed across the contributions of all regions) are both about 0.32 W/m^2 for BC, -0.10 W/m^2 for POA, and -0.48 W/m^2 for SIOA, comparable to the mean values estimated in the IPCC AR5 (0.40 W/m^2, -0.09 W/m^2 and -0.51 W/m^2, respectively)[1]. [Note that although the IPCC AR5 values are for the anthropogenic aerosol changes from 1750 to 2011, the anthropogenic emissions are negligible in 1750[73,92], and the changes from 2007 to 2011 are very small[1].] Here we provide a general discussion of errors in emissions, CTM and RTM relevant to the global and regional RF and the relative difference between regional RF_c and RF_p. All errors are referred to as 2σ uncertainties that correspond to a 95% confidence interval (CI) – for example, an error of 10% for a best estimate of 1.0 means a 95% CI at [0.9, 1.1].

The calculation of E_p is subject to errors in national production data and emission factors[13,14,58]. The HTAP assessment report[91] suggests a lower bound of errors in the global total E_p to be 10–30% for the species studied here. Regionally, E_p may contain larger errors in the developing countries due to less accurate data inputs; this additional error is estimated here to be within 30%, by comparing E_p for the 11 individual regions between the HTAP v2.2 inventory and our results.

Regionally, E_c shares most errors with E_p, although E_c contains an additional error from the MRIO calculation[13,18] associated with inaccuracies in national economic statistics, sectoral details and data harmonization[93,94]. Peters et al.[31] showed that regional E_p and E_c of CO_2 have comparable variability across studies that use different MRIO models, suggesting a very small MRIO-related error compared to the error in E_p. The study on China's trade with a detailed statistical analysis by Lin et al.[13] showed that the uncertainty in the input-output analysis contributes ~ 10% of total errors in export-related emissions of pollutants, with the remaining 90% from the calculation of E_p. Considering the MRIO-related error, here we assume a 10% additive error for E_c on top of the error translated from E_p. This leads to the 2σ error values (calculated as 10% * E_c / E_p) presented in Fig. 1.

Given the amount of emissions, the RF calculation is subject to errors in the CTM-simulated atmospheric processes[65,91] and the RTM-simulated radiative transfer processes. The atmospheric loadings and vertical profiles of aerosols are relatively well simulated by the CTM here[73,95]. Larger uncertainties exist in the current understanding of aerosol optical properties[2,3,73], such as the extent of absorption enhancement of BC

through internal mixing[2] and the absorption capability of POA[96]. The CTM and RTM related errors together are on the order of 30% for SIOA, 50% for POA, and 100% for BC[2,73,95,97].

It is computationally prohibitive to perform systematic Monte Carlo or sensitivity analyses that integrate all errors associated with emissions, CTM and RTM. Here we give a rough estimate. Globally accumulated RF_p and RF_c share the same errors, and we estimate an error of 40% for SIOA, 60% for POA, and 150% for BC (i.e., by a factor of 2.5), based on the uncertainties adopted in the IPCC AR5[1]. The errors for regional RF_p and RF_c may be larger for less-studied developing regions. Nevertheless, most errors in regional RF_p and RF_c are common and do not affect their relative difference[13], except for the effect of MRIO-related error on RF_c (inherited from E_c). To account for the MRIO-related error, we assume a 10% additive error for regional RF_c on top of the error translated from RF_p. This leads to the 2σ error values (calculated as 10% * RF_c / RF_p) presented in Fig. 3.

Due to lack of data, we do not consider the impact of trade on aerosols related to international aviation or shipping. Nor do we include secondary organic aerosols because of considerable difficulties and uncertainties in emission calculations and chemical simulations. Although some portions of POA may absorb the solar radiation and partly (by 27%) offset the negative RF by POA scattering[96], we do not account for this absorption due to large uncertainties in determining the absorbing POA, consistent with the IPCC AR5 assumption. We also do not quantify the indirect RF of aerosols. Inclusion of these aspects would reveal additional effects of trade on aerosol RF.

References

32 Bond, T. C. *et al.* A technology-based global inventory of black and organic carbon emissions from combustion. *Journal of Geophysical Research* **109**, D14203 (2004).

33 Zhang, Q. *et al.* Asian emissions in 2006 for the NASA INTEX-B mission. *Atmospheric Chemistry and Physics* **9**, 5131-5153 (2009).

34 Streets, D. *et al.* An inventory of gaseous and primary aerosol emissions in Asia in the year 2000. *Journal of Geophysical Research* **108**, D21, 8809 (2003).

35 IEA. *Energy Statistics and Balances of OECD Countries, 2007-2008* (International Energy Agency, 2010).

36 IEA. *Energy Statistics and Balances of Non-OECD Countries, 2007-2008* (International Energy Agency, 2010).

37 Liu, F. *et al.* High-resolution inventory of technologies, activities, and emissions of coal-fired power plants in China from 1990 to 2010. *Atmospheric Chemistry and Physics* **15**, 13299-13317 (2015).

38 Yan, F., Winijkul, E., Jung, S., Bond, T. C. & Streets, D. G. Global emission projections of particulate matter (PM): I. Exhaust emissions from on-road vehicles. *Atmospheric Environment* **45**, 4830-4844 (2011).

39 Yan, F. *et al.* Global emission projections for the transportation sector using dynamic technology modeling. *Atmospheric Chemistry and Physics* **14**, 5709-5733 (2014).

40 Lu, Z. *et al.* Sulfur dioxide emissions in China and sulfur trends in East Asia since 2000. *Atmospheric Chemistry and Physics* **10**, 6311-6331 (2010).

41 Streets, D. G., Wu, Y. & Chin, M. Two-decadal aerosol trends as a likely explanation of the global dimming/brightening transition. *Geophysical Research Letters* **33**, L15806(2006).

42 Streets, D. G. *et al.* Anthropogenic and natural contributions to regional trends in aerosol optical depth, 1980-2006. *Journal of Geophysical Research; Atmospheres* **114**, D00D18(2009).

43 Streets, D. G. *et al.* Aerosol trends over China, 1980-2000. *Atmospheric Research* **88**, 174-182 (2008).

44 EMEP. EMEP/EEA Air Pollutant Emission Inventory Guidebook 2013: Technical Guidance to Prepare National EmissionInventories. (2013).

45 USEPA. Compilation of Air Pollutant Emission Factors (AP-42). U.S. Environmental Protection Agency. (1999).

46 Lei, Y., Zhang, Q., He, K. B. & Streets, D. G. Primary anthropogenic aerosol emission trends for China, 1990-2005. *Atmospheric Chemistry and Physics* **11**, 931-954 (2011).

47 Lu, Z. & Streets, D. G. The Southeast Asia Composition, Cloud, Climate Coupling Regional Study Emission Inventory, available at: http://bio.cgrer.uiowa.edu/SEAC4RS/emission.html (last access: 26 March 2014), (2012).

48 Olivier, J. *et al.* Applications of EDGAR Emission Database for Global Atmospheric Research. *Rijksinstituut Voor Volksgezondheid En Milieu Rivm* (2002).

49 Zhang, Q. *et al.* NOx emission trends for China, 1995–2004: The view from the ground and the view from space. *Journal of Geophysical Research* **112**, D22306 (2007).

50 Kurokawa, J. *et al.* Emissions of air pollutants and greenhouse gases over Asian regions during 2000–2008: Regional Emission inventory in ASia (REAS) version 2. *Atmospheric Chemistry and Physics* **13**, 11019-11058 (2013).

51 Lu, Z. F. & Streets, D. G. Increase in NOx Emissions from Indian Thermal Power Plants during 1996-2010: Unit-Based Inventories and Multisatellite Observations. *Environmental Science & Technology* **46**, 7463-7470 (2012).

52 Vestreng, V. *et al.* Evolution of NOx emissions in Europe with focus on road transport control measures. *Atmospheric Chemistry and Physics* **9**, 1503-1520 (2009).

53 Yevich, R. & Logan, J. A. An assessment of biofuel use and burning of agricultural waste in the developing world. *Global Biogeochemical Cycles* **17**, 1095(2003).

54 Bond, T. C. *et al.* Historical emissions of black and organic carbon aerosol from energy-related combustion, 1850-2000. *Global Biogeochemical Cycles* **21**, GB2018 (2007).

55 Lam, N. L. *et al.* Household Light Makes Global Heat: High Black Carbon Emissions From Kerosene Wick Lamps. *Environmental Science & Technology* **46**, 13531-13538 (2012).

56 Huang, Y. *et al.* Global organic carbon emissions from primary sources from 1960 to 2009. *Atmospheric Environment* **122**, 505-512 (2015).

57 Janssens-Maenhout, G. *et al.* HTAP_v2.2: a mosaic of regional and global emission gridmaps for 2008 and 2010 to study hemispheric transport of air pollution. *Atmospheric Chemistry and Physics* **15**, 12867-12909 (2015).

58 Janssens-Maenhout, G., Petrescu, A. M. R., Muntean, M. & Blujdea, V. *Verifying Greenhouse Gas Emissions: Methods to Support International Climate Agreements*. (The National Academies Press, 2010).

59 Janssens-Maenhout, G. *et al. EDGAR-HTAP: A Harmonized Gridded Air Pollution Emission Dataset Based on national inventories*. (Publications Office, 2011).

60 Davis, S. J. & Caldeira, K. Consumption-based accounting of CO2 emissions. *Proceedings of the National Academy of Sciences* **107**, 5687-5692 (2010).

61 Feng, K. *et al.* Outsourcing CO_2 within China. *Proceedings of the National Academy of Sciences USA* **110**, 11654-11659 (2013).

62 Lininger, C. in *Consumption-Based Approaches in International Climate Policy* Vol. 6 91-113 (Springer International Publishing, 2015).

63 Wiedmann, T. in *Taking Stock of Industrial Ecology* Vol. 8 159-180 (Springer International Publishing, 2016).

64 Mao, J. *et al.* Ozone and organic nitrates over the eastern United States: Sensitivity to isoprene chemistry. *Journal of Geophysical Research: Atmospheres* **118**, 11256-211268 (2013).

65 Yan, Y.-Y., Lin, J.-T., Chen, J. & Hu, L. Improved simulation of tropospheric ozone by a global-multi-regional two-way coupling model system. *Atmospheric Chemistry and Physics* **16**, 2381-2400 (2016).

66 Park, R. J., Jacob, D. J., Field, B. D., Yantosca, R. M. & Chin, M. Natural and transboundary pollution influences on sulfate-nitrate-ammonium aerosols in the United States: Implications for policy. *Journal of Geophysical Research: Atmospheres* **109**, D15204 (2004).

67 Park, R. J., Jacob, D. J., Kumar, N. & Yantosca, R. M. Regional visibility statistics in the United States: Natural and transboundary pollution influences, and implications for the Regional Haze Rule. *Atmospheric Environment* **40**, 5405-5423 (2006).

68 Park, R. J., Jacob, D. J., Chin, M. & Martin, R. V. Sources of carbonaceous aerosols over the United States and implications for natural visibility. *Journal of Geophysical Research: Atmospheres* **108**, D12, 4355 (2003).

69 Fairlie, T. D. *et al.* Impact of mineral dust on nitrate, sulfate, and ozone in transpacific Asian pollution plumes. *Atmospheric Chemistry and Physics* **10**, 3999-4012 (2010).

70 Zender, C. S., Bian, H. S. & Newman, D. Mineral Dust Entrainment and Deposition (DEAD) model: Description and 1990s dust climatology. *Journal of Geophysical Research: Atmospheres* **108**, D14, 4416 (2003).

71 Jaeglé, L., Quinn, P. K., Bates, T. S., Alexander, B. & Lin, J. T. Global distribution of sea salt aerosols: new constraints from in situ and remote sensing observations. *Atmospheric Chemistry and Physics* **11**, 3137-3157.

72 Alexander, B. *et al.* Sulfate formation in sea-salt aerosols: Constraints from oxygen isotopes. *Journal of Geophysical Research: Atmospheres* **110**, D10307 (2005).

73 Heald, C. L. *et al.* Contrasting the direct radiative effect and direct radiative forcing of aerosols. *Atmospheric Chemistry and Physics* **14**, 5513-5527 (2014).

74 Fountoukis, C. & Nenes, A. ISORROPIA II: a computationally efficient thermodynamic equilibrium model for K+-Ca2+-Mg2+-Nh(4)(+)-Na+-SO42--NO3--Cl--H2O aerosols. *Atmospheric Chemistry and Physics* **7**, 4639-4659 (2007).

75 Liu, H., Jacob, D. J., Bey, I. & Yantosca, R. M. Constraints from 210Pb and 7Be on wet deposition and transport in a global three-dimensional chemical tracer model driven by assimilated meteorological fields. *Journal of Geophysical Research* **106**, 12109-12112,12128 (2001).

76 Wang, Q. *et al.* Sources of carbonaceous aerosols and deposited black carbon in the Arctic in winter-spring: implications for radiative forcing. *Atmospheric Chemistry and Physics* **11**, 12453-12473 (2011).

77 Wesely, M. L. Parameterization of surface resistances to gaseous dry deposition in regional-scale numerical models. *Atmospheric Environment* **23**, 1293-1304 (1989).

78 Zhang, L., Gong, S., Padro, J. & Barrie, L. A size-segregated particle dry deposition scheme for an atmospheric aerosol module. *Atmospheric Environment* **35**, 549-560 (2001).

79 Lin, S.-J. & Rood, R. B. Multidimensional flux-form semi-Lagrangian transport schemes. *Monthly Weather Review* **124**, 2046-2070 (1996).

80 Rienecker, M. M. *et al.* The GEOS-5 Data Assimilation System—Documentation of Versions 5.0.1, 5.1.0, and 5.2.0. 118 (2008).

81 Holtslag, A. & Boville, B. Local versus nonlocal boundary-layer diffusion in a global climate model. *Journal of Climate* **6**, 1825-1842 (1993).

82 Lin, J.-T. & McElroy, M. B. Impacts of boundary layer mixing on pollutant vertical profiles in the lower troposphere: Implications to satellite remote sensing. *Atmospheric Environment* **44**, 1726-1739 (2010).

83 Hu, L. *et al.* Emissions of C6–C8 aromatic compounds in the United States: Constraints from tall tower and aircraft measurements. *Journal of Geophysical Research: Atmospheres* **120**, 826-842 (2015).

84 Guenther, A. *et al.* The Model of Emissions of Gases and Aerosols from Nature version 2.1 (MEGAN2. 1): an extended and updated framework for modeling biogenic emissions. *Geoscientific Model Development* **5**, 1471-1492 (2012).

85 Hudman, R. C. *et al.* Steps towards a mechanistic model of global soil nitric oxide emissions: implementation and space based-constraints. *Atmospheric Chemistry and Physics* **12**, 7779-7795 (2011).

86 Price, C. & Rind, D. A simple lightning parameterization for calculating global lightning distributions. *Journal of Geophysical Research: Atmospheres (1984–2012)* **97**, 9919-9933 (1992).

87 Murray, L. T., Jacob, D. J., Logan, J. A., Hudman, R. C. & Koshak, W. J. Optimized regional and interannual variability of lightning in a global chemical transport model constrained by LIS/OTD satellite data. *Journal of Geophysical Research: Atmospheres* **117**, D20307 (2012).

88 Ott, L. E. *et al.* Production of lightning NO(x) and its vertical distribution calculated from three-dimensional cloud-scale chemical transport model simulations. *Journal of Geophysical Research: Atmospheres* **115**, D04301 (2010).

89 van der Werf, G. R. *et al.* Global fire emissions and the contribution of deforestation, savanna, forest, agricultural, and peat fires (1997–2009). *Atmospheric Chemistry and Physics* **10**, 11707-11735 (2010).

90 Iacono, M. J. *et al.* Radiative forcing by long−lived greenhouse gases: Calculations with the AER radiative transfer models. *Journal of Geophysical Research: Atmospheres (1984–2012)* **113**, D13103 (2008).

91 HTAP. Hemispheric transport of air pollution 2010 Part A: Ozone and particulate matter. (Economic Commission for Europe, Geneva, 2010).

92 Dentener, F. *et al.* Emissions of primary aerosol and precursor gases in the years 2000 and 1750 prescribed data-sets for AeroCom. *Atmospheric Chemistry and Physics* **6**, 4321-4344 (2006).

93 Wiedmann, T., Wilting, H. C., Lenzen, M., Lutter, S. & Palm, V. Quo Vadis MRIO? Methodological, data and institutional requirements for multi-region input–output analysis. *Ecological Economics* **70**, 1937-1945 (2011).

94 Tukker, A. & Dietzenbacher, E. Global multiregional input-output frameworks: an introduction and outlook. *Economic Systems Research* **25**, 1-19 (2013).

95 Wang, Q. *et al.* Global budget and radiative forcing of black carbon aerosol: Constraints from pole-to-pole (HIPPO) observations across the Pacific. *Journal of Geophysical Research: Atmospheres* **119**, 195-206 (2014).

96 Lu, Z. *et al.* Light Absorption Properties and Radiative Effects of Primary Organic Aerosol Emissions. *Environmental Science & Technology* **49**, 4868-4877 (2015).

97 Myhre, G. *et al.* Radiative forcing of the direct aerosol effect from AeroCom Phase II simulations. *Atmospheric Chemistry and Physics* **13**, 1853-1877 (2013).

98 Paulot, F. *et al.* Ammonia emissions in the United States, European Union, and China derived by high‐resolution inversion of ammonium wet deposition data: Interpretation with a new agricultural emissions inventory (MASAGE_NH3). *Journal of Geophysical Research* **119**, 4343-4364 (2014).

99 EPA. The 2008 National Emissions Inventory (NEI), release v3. (2013).

100 Huang, X. *et al.* A high‐resolution ammonia emission inventory in China. *Global Biogeochemical Cycles* **26**, GB1030 (2012).

101 EMEP. EMEP/CEIP 2014 Present state of emission data. (2014).

102 Environmental-Canada. The National Pollutant Release Inventory (NPRI). (2015).

103 JRC/PBL. Emission Database for Global Atmospheric Research (EDGAR), release EDGARv4.2 FT2010. (2013).

Supplementary Information Tables

Supplementary Information Table 1 | Global RF of SIOA, POAand BC. Radiative forcing of aerosols calculated from three methods: excluding global anthropogenic emissions (with respect to cases R2–R4 for SIOA, POAand BC, respectively, first row), excluding production-based anthropogenic emissions of the 11 regions one by one (cases R5–R37, second row), and excluding consumption-based anthropogenic emissions of the 11 regions one by one (cases R38–R70, third row).

	SIOA	POA	BC
All	-0.481	-0.0990	0.326
Production	-0.486	-0.0984	0.324
Consumption	-0.492	-0.0984	0.324

Supplementary Information Table 2 | Emission Inventories used in this study for NH_3

Region	Agriculture (number of sectors)	Other activities (number of sectors)
Contiguous United States	MASAGE (27), ref [98]	NEI (53), ref [99]
China	MASAGE (27), ref [98]	Huang et al. (5), ref [100]
Europe	EMEP (19), ref [101]	EMEP (93), ref [101]
Rest of Asia	REAS (1), ref [50]	REAS (19), ref [50]
Canada	NPRI (4), ref [102]	NPRI (113), ref [102]
Other regions	EDGAR (3), ref [103]	EDGAR (17), ref [103]

Supplementary Information Figures

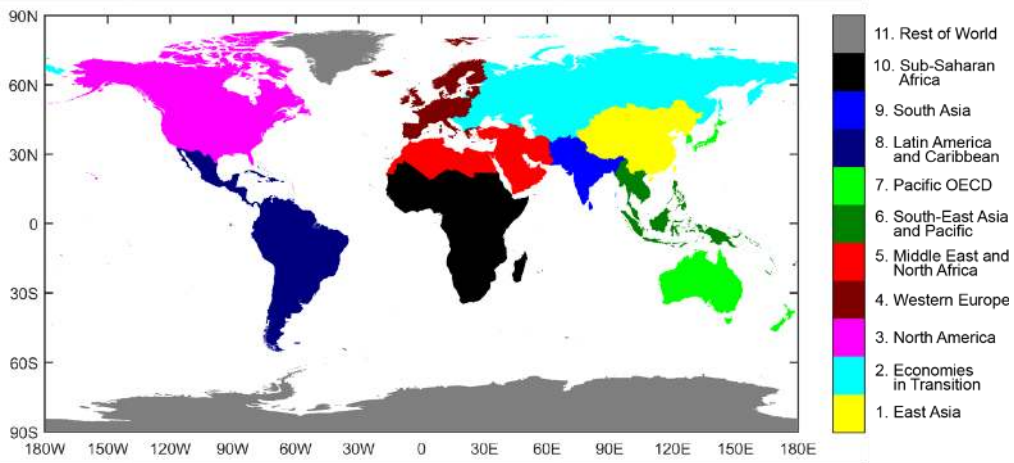

Supplementary Information Figure 1 | Map of 11 key regions analyzed here. The definition of the first 10 regions follows the IPCC AR5 Working Group 3 Report Chapter 14[16], except that South Korea is included in the Pacific OECD region instead of East Asia region.

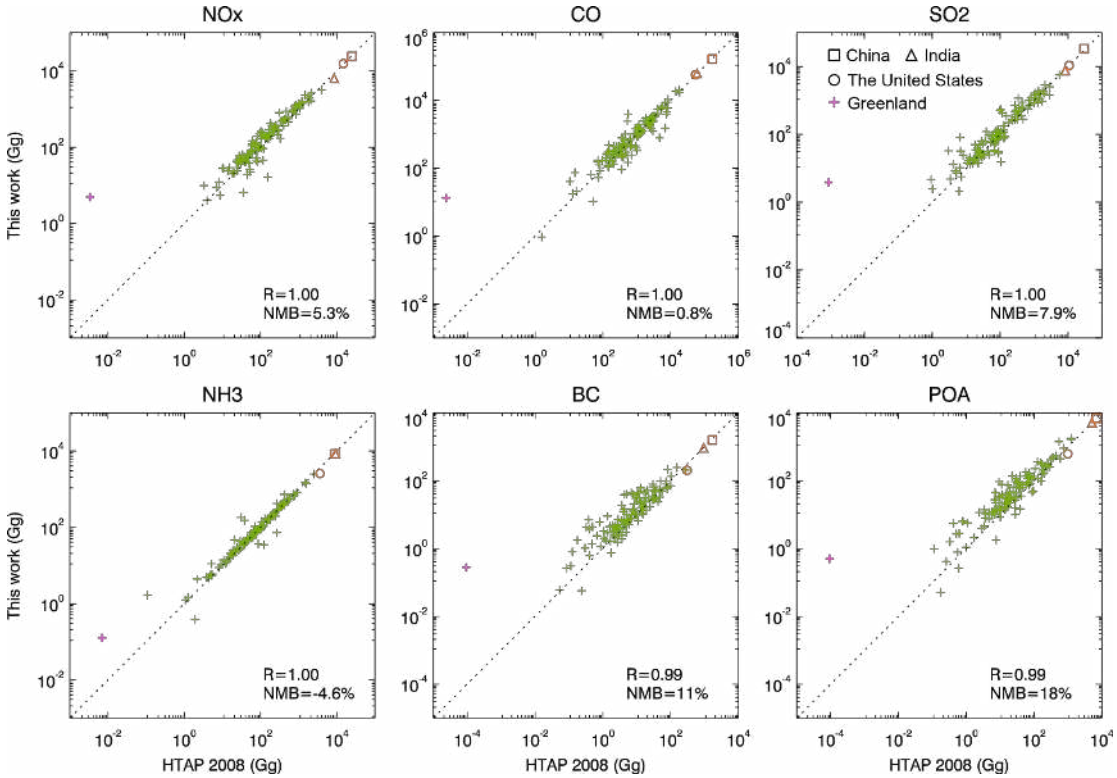

Supplementary Information Figure 2 | Scatterplot for E_p between this work and the HTAP v2.2 inventory for 2008. Data are displayed in logarithmic scale for better illustration of small values. In each panel, the correlation (r) and normalized mean bias are also given. The three largest emitters, China, India and the United States, are indicated by special symbols, and the outlier region, Greenland, is indicated in pink.

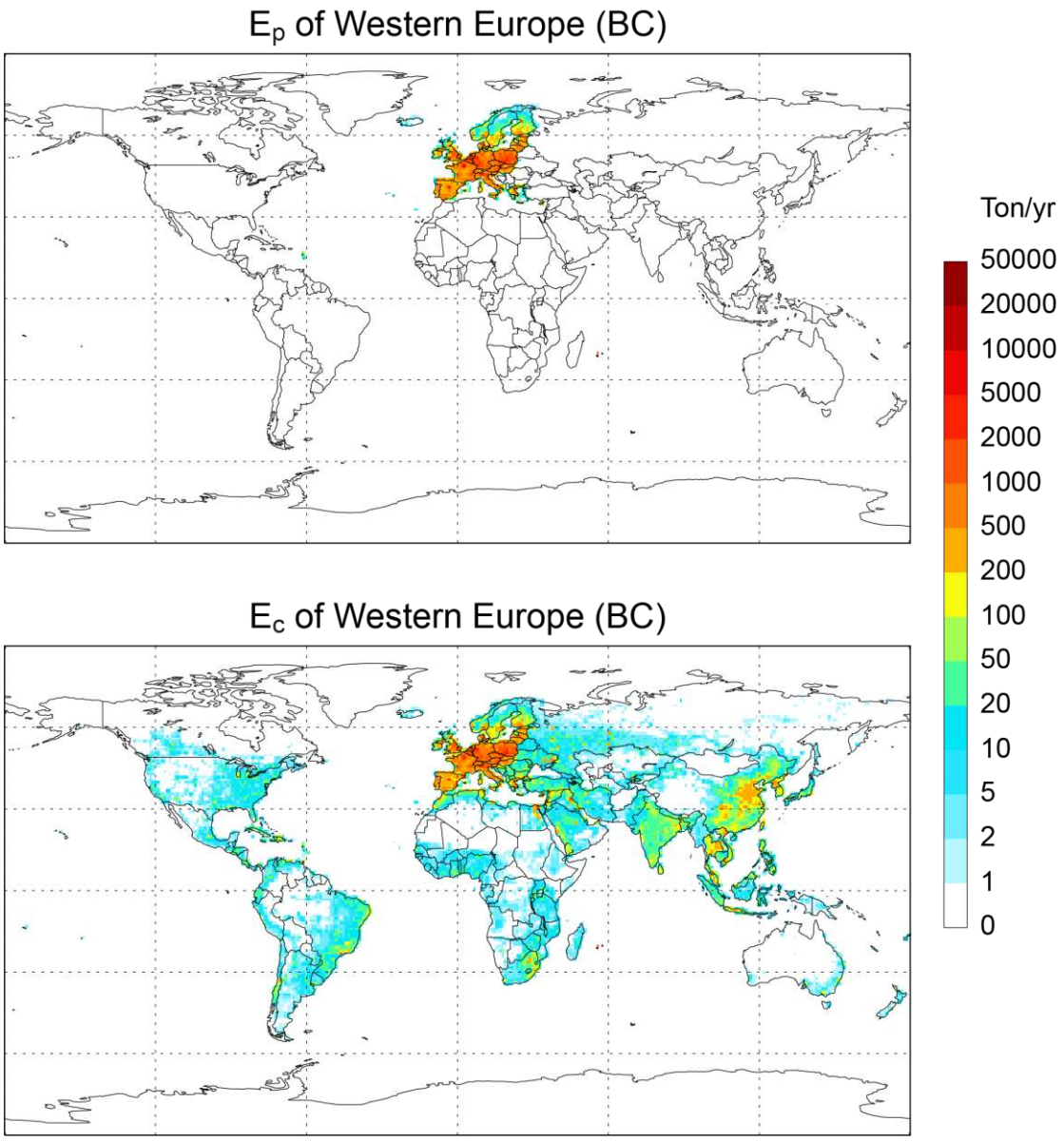

Supplementary Information Figure 3 | Spatial distributions of Western Europe's E_p and E_c for black carbon.

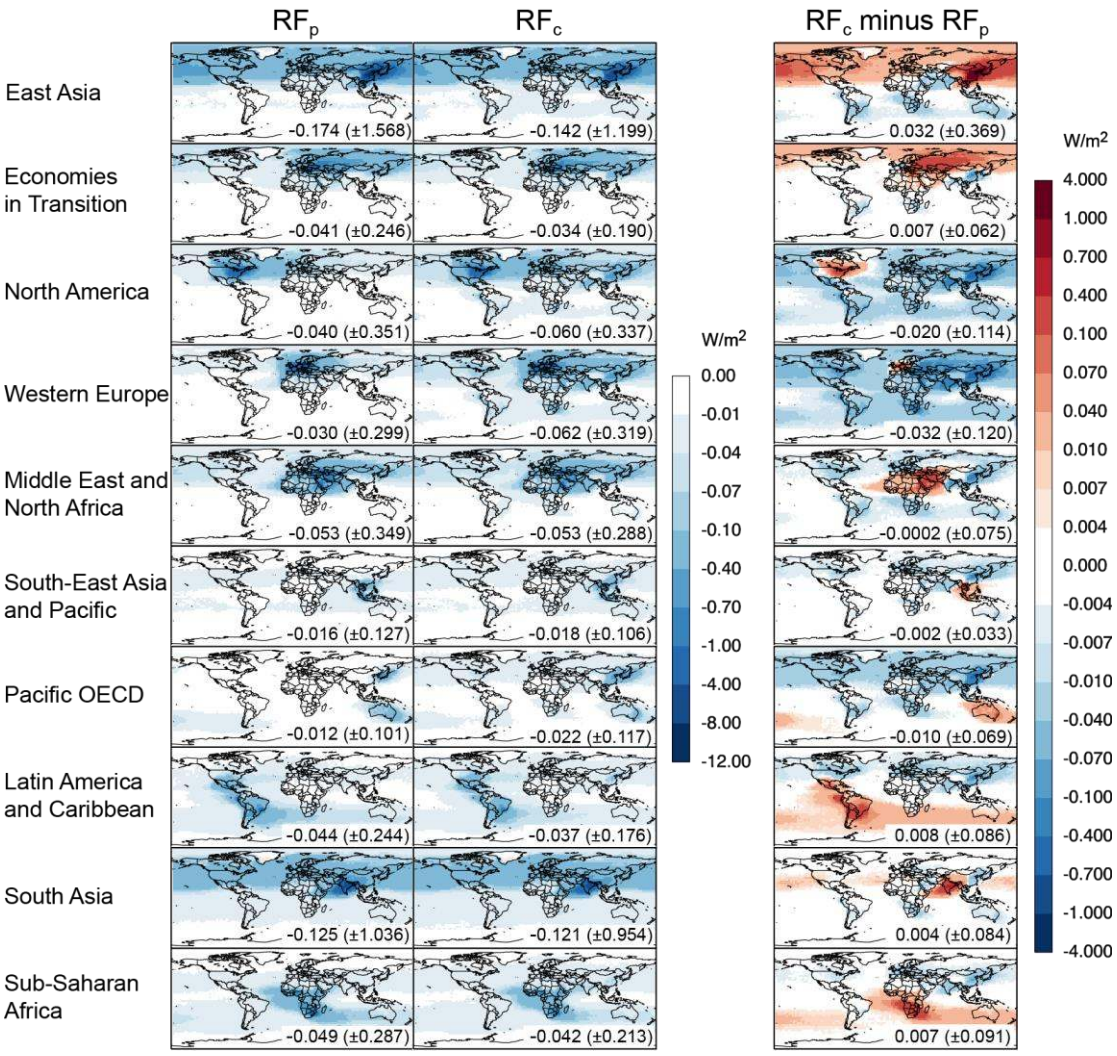

Supplementary Information Figure 4 | Spatial distribution of production- and consumption-based radiative forcing and their difference for SIOA+POA contributed by individual regions. The RF contributed by Rest of the World is very small and omitted here. The numbers in each panel indicate the spatial mean and standard deviation. The color scales are consistent in Supplementary Information Figs. 4-6.

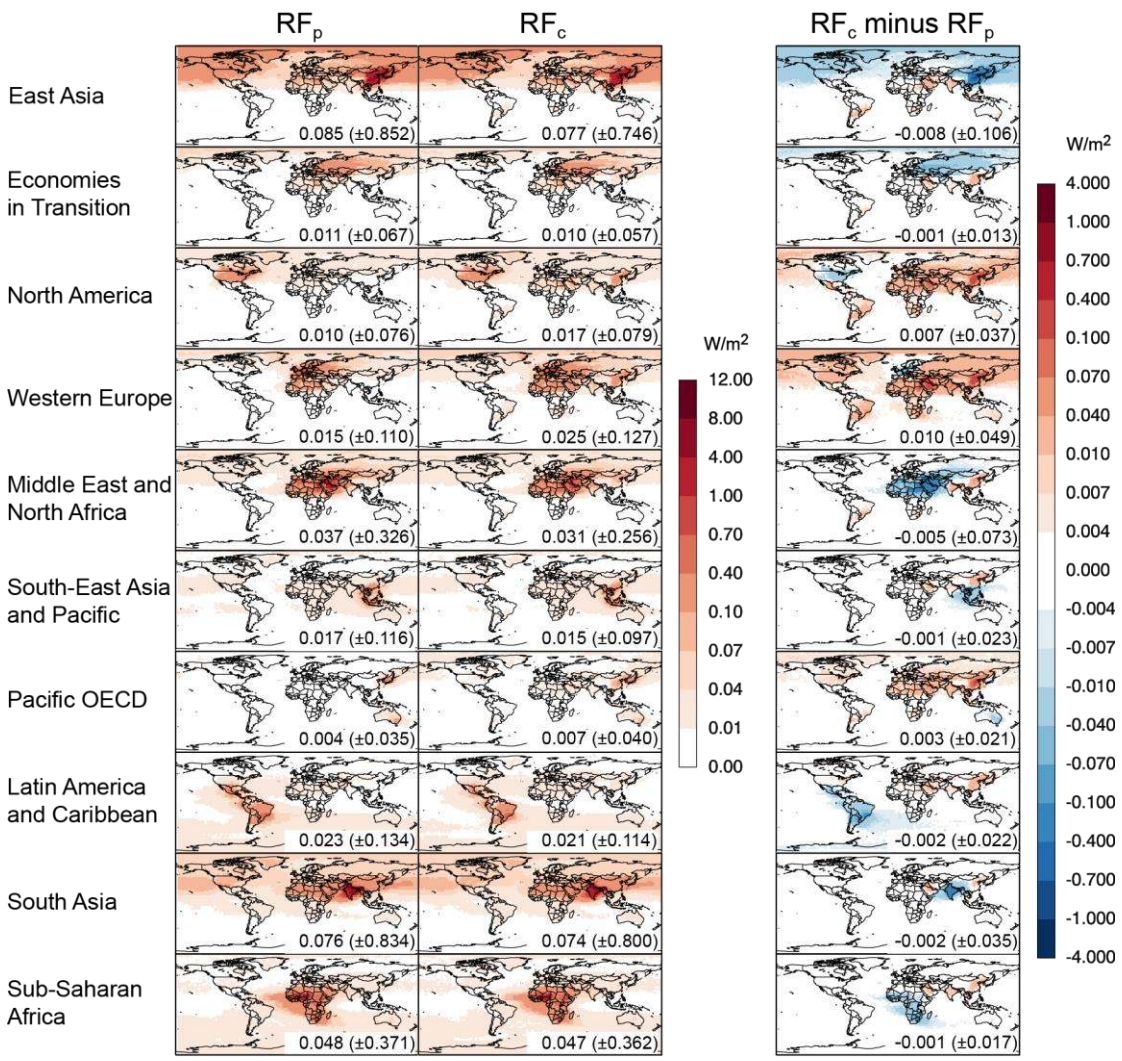

Supplementary Information Figure 5 | Spatial distribution of production- and consumption-based radiative forcing and their difference for BC contributed by individual regions. The RF contributed by Rest of the World is very small and omitted here. The numbers in each panel indicate the spatial mean and standard deviation. The color scales are consistent in Supplementary Information Figs. 4-6.

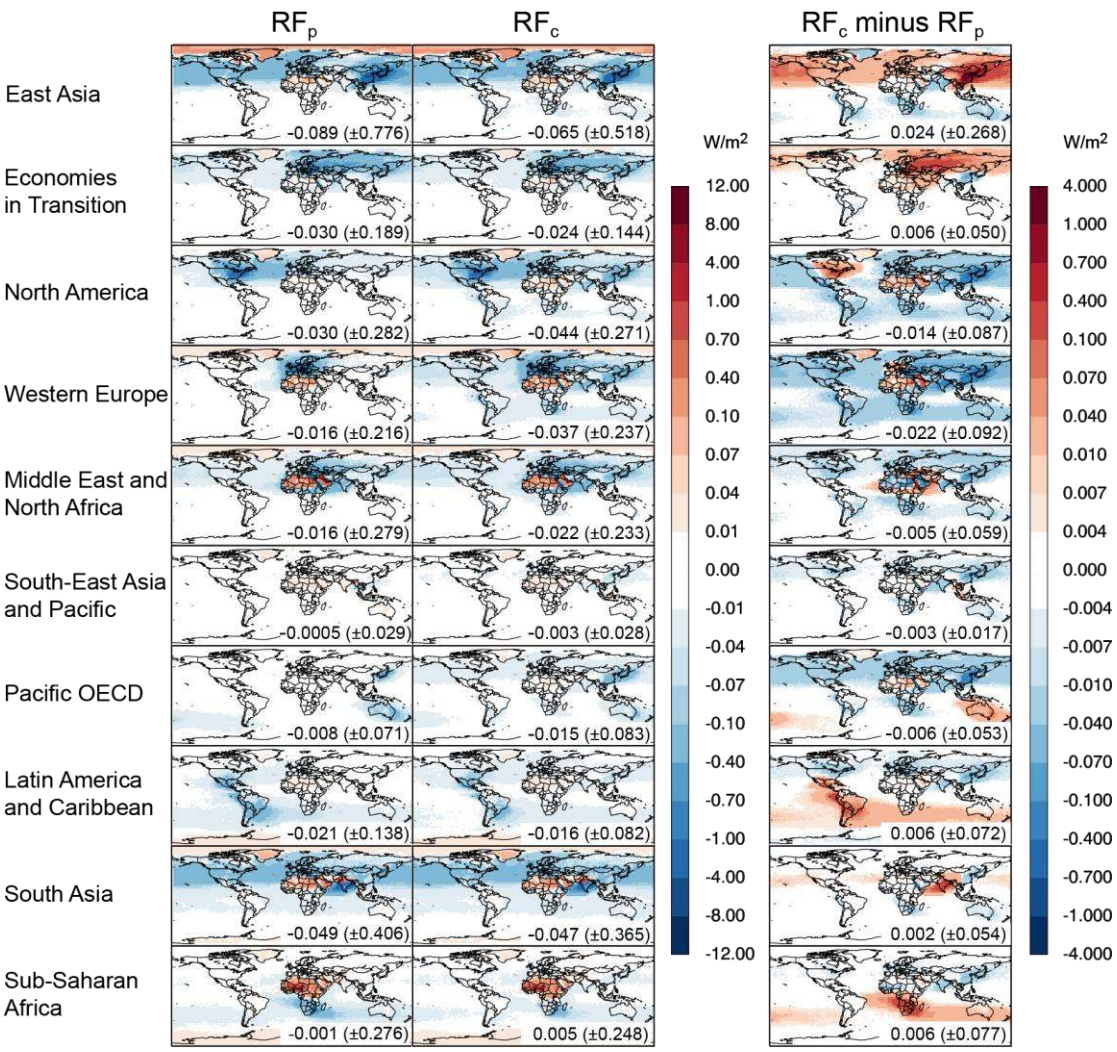

Supplementary Information Figure 6 | Spatial distribution of production- and consumption-based radiative forcing and their difference for SIOA+POA+BC contributed by individual regions. The RF contributed by Rest of the World is very small and omitted here. The numbers in each panel indicate the spatial mean and standard deviation. The color scales are consistent in Supplementary Information Figs. 4-6.

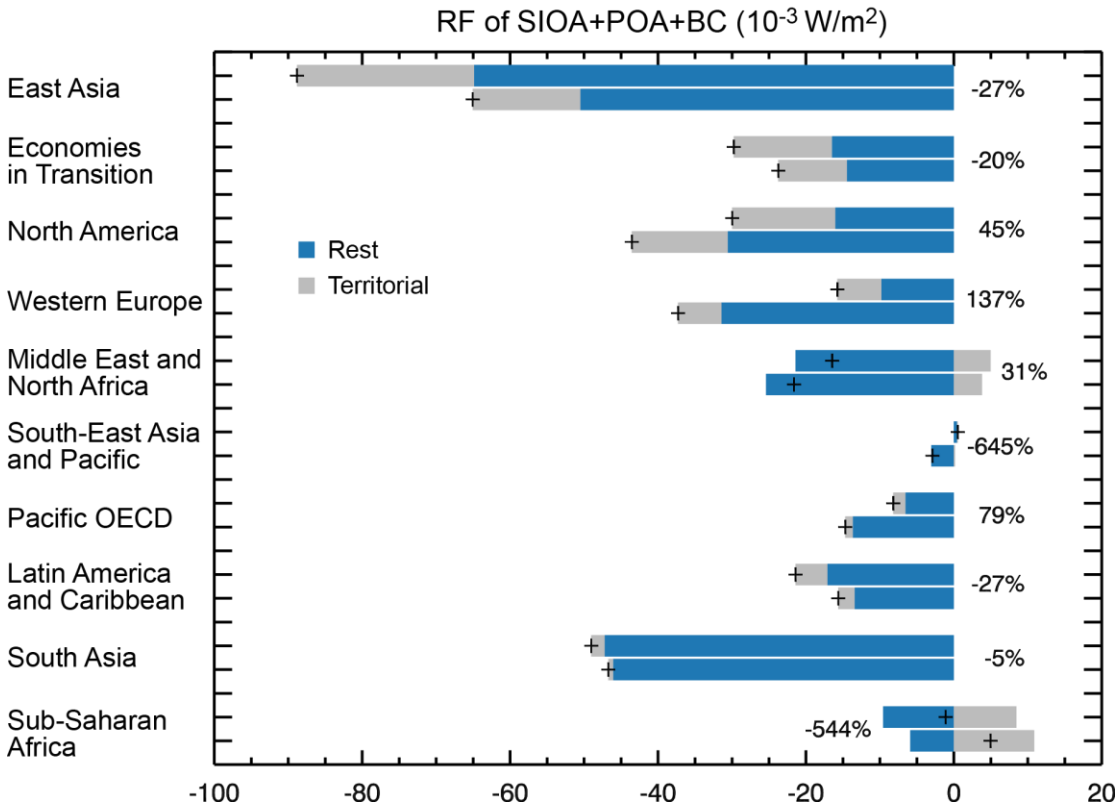

Supplementary Information Figure 7 | Global production- and consumption-based radiative forcing of SIOA+POA+BC for the 11 regions. Net RF_p (upper bar) and RF_c (lower bar) of SIOA+POA+BC contributed by individual regions ('+' symbol), summed from the RF imposed above (grey bar) and outside (blue bar) their territories. For a given region, the percentage value indicates the relative change from RF_p to RF_c. For South-East Asia and Pacific, the RF_p imposed outside that region is positive; and the RF_p above that region is close to zero and invisible from the figure. For Sub-Saharan Africa, the RF_c imposed outside that region is negative, but it is more than offset by the positive RF_c imposed above that region.

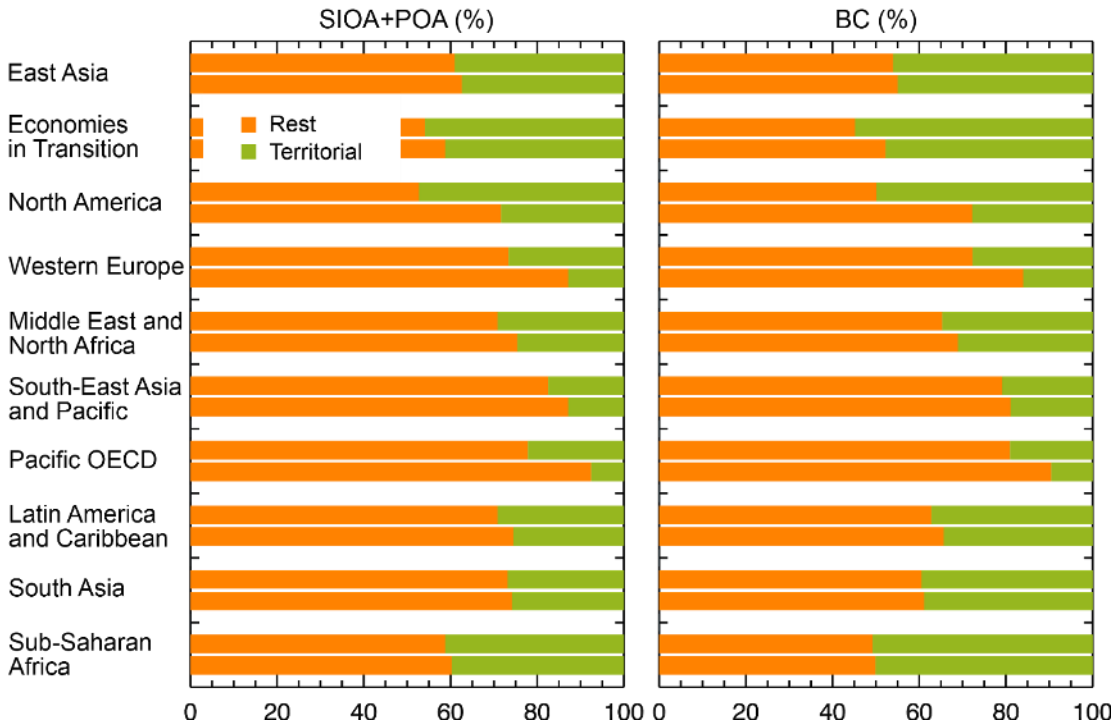

Supplementary Information Figure 8 | Percentage fraction of aerosol mass within and outside each region. For the global aerosol mass related to a given region's production (upper bar) or consumption (lower bar), the percentages of aerosol mass above (green bar) and outside (orange bar) the given region.

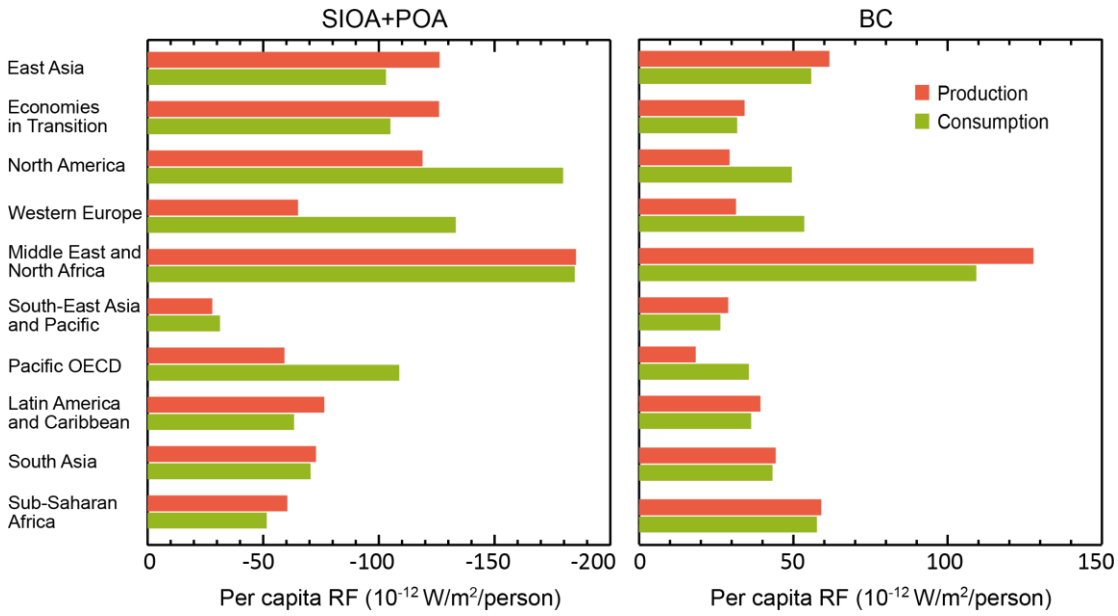

Supplementary Information Figure 9 | Production- and consumption-based radiative forcing of SIOA+POA and BC on a per capita basis.